Opal Circuits of Light—Planarized Microphotonic Crystal Chips**

By *San Ming Yang*, *Hernán Míguez*, and *Geoffrey A. Ozin**

We present a novel technique coined directed evaporation-induced self-assembly (DEISA) that enables the formation of planarized opal-based microphotonic crystal chips in which opal crystal shape, size, and orientation are under synthetic control. We provide detailed synthetic protocols that underpin the DEISA process and formulate directed self-assembly strategies that are suited for the fabrication of opal architectures with complex form and designed optical functionality. These developments bode well for the utilization of opal-based photonic crystals in microphotonic crystal devices and chips.

1. Introduction

Self-assembly of monodisperse microspheres to create 3D opal structures is a simple and inexpensive approach to the fabrication of photonic crystals.[1–3] However, in order to integrate these synthetic opal crystals into microphotonic crystal devices they have to be fashioned in the form of optically functional planarized architectures, which can behave as switches, mirrors, filters, waveguides, lasers, or superprisms.[4–7] This is an achievable goal provided simple and reproducible methods can be devised to shape opal lattices into planarized microphotonic crystal components that have precise control over crystal size, shape, and orientation with a sufficiently high level of microstructural perfection and optical quality with minimal light losses for envisioned optical telecommunication applications.[8]

In this paper we present synthetic details on the preparation of opal crystal architectures with complex form that offer optical functionality and quality, which make them potentially suitable for applications in microphotonic crystal devices and chips. The approach utilizes a collection of strategies in confined microsphere crystallization and soft lithography and its versatility and effectiveness are demonstrated by reference to the construction of a) uniform and modulated thickness opal microchannels with a rectangular cross section and b) modulated lattice dimension opal microchannels. While the focus of this paper is purely synthesis, it is important to note that in related papers from this laboratory, detailed optical microscope spectroscopy studies of opals with complex form have demonstrated their high optical quality, the capacity to crystal engineer their photonic crystal properties, and their ability to function as tunable optical Bragg filters and mirrors.

[*] Prof. G. A. Ozin, Dr. S. M. Yang, Dr. H. Míguez
Materials Chemistry Research Group, Department of Chemistry
University of Toronto
80 St. George Street, Toronto, Ontario, M5S 3H6 (Canada)
E-mail: gozin@alchemy.chem.utoronto.ca.

[**] GAO is Government of Canada Research Chair in Materials Chemistry. The microphotonic crystal research of the materials chemistry research group at the University of Toronto has been generously financed by the Natural Sciences and Engineering Research Council of Canada, the Connaught Foundation, and the University of Toronto. The authors are indebted to the Univesity of Alberta for access to Microfab.

2. Results and Discussion

In the following sections we will describe a novel self-assembly technique coined directed evaporation induced self-assembly (DEISA), shown in Figure 1, to synthesize, for example, parallel arrays of opal microchannels of uniform thickness and rectangular cross section that are either housed on the surface or buried within a substrate.

Fig. 1. DEISA in action: a graphical representation of opal crystal formation inside rectangular-shaped microchannels on a flat substrate.

2.1. Microchannel Template

To create surface-supported or -confined opal microchannels it is first necessary to make a suitable microchannel template. One way of making the template employs micromolding inside microcapillaries (MIMIC)[9] whereby a poly(dimethylsiloxane) (PDMS) elastomeric stamp patterned with a parallel array of micrometer-scale rectangular-shaped microchannels is used as a master. Since the rectangular channel pattern as shown in Figure 2a is a replica structure of the PDMS pattern, the channel depth on the substrate is controlled by the photoresist thickness on the original silicon master. Instead of the micromolding method to build vertical wall microchannels on flat substrates, another way to create vertical wall grooves buried

  1616-301X/02/0706-0425 $ 17.50+.50/0

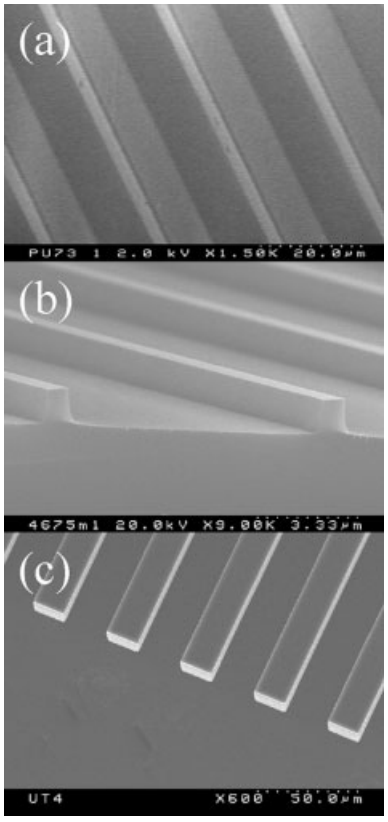

Fig. 2. Representative SEM images of rectangular-shaped microchannels prepared by a) micromolding of polyurethane, b) anisotropic etching of a Si <100> wafer, c) DRIE of a Si <100> wafer.

within the surface of a Si wafer surface is through microcontact printing and anisotropic Si etching.[9] In this case, a line-patterned PDMS stamp is used to print a hexadecanethiol monolayer on a gold-coated Si wafer (50 nm Au/5 nm Ti/Si(100)). The line pattern is printed at 45° with respect to the flat reference end of the wafer. The bare gold and underlying titanium are subsequently etched away and then the silicon substrate is etched using a potassium hydroxide solution (KOH 65–70 wt.-% in H_2O/isopropanol) at 70–80 °C. At this high KOH concentration and reaction temperature the etching rate of the {100} face of silicon is slower than that of {110} and enables the formation of a silicon surface relief pattern of vertical wall microchannels with a rectangular cross section as seen in Figure 2b.[10] In addition to the wet chemical method, vertical wall rectangular-shaped microchannels buried within the surface of a silicon wafer can be created by deep reactive ion etching (RIE) (Bosch process). The resulting silicon surface relief pattern of parallel microchannels with rectangular cross section are shown in Figure 2c.

2.2. Opal Microchannels—Uniform Thickness

The microchannel template made by the aforementioned methods is immersed in a vertical orientation into a dispersion of monodisperse silica microspheres, Figure 1. The choice of dispersant depends on its volatility at room temperature, preferably water or short-chain alcohols (carbon number = 1 to 4) are used. In ethanol, for example, the microspheres spontaneously self-assemble and crystallize as well-ordered opal single crystals exclusively inside the rectangular-shaped microchannels. This kind of localized crystallization of opals likely occurs because of strong capillary-driven directional mass flow of microspheres from the dispersion exclusively into the spatial confines of the microchannels and not on the top surfaces of the adjacent dividing walls as seen in Figure 3a. Colloidal interactions and capillary forces between microspheres as well as

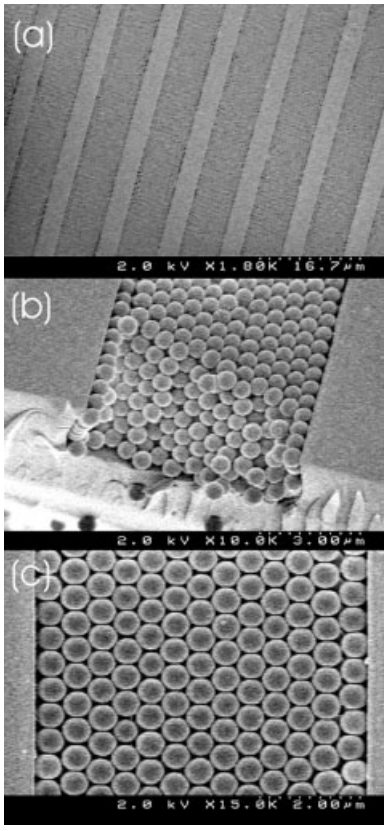

Fig. 3. Representative SEM images of micrometer-scale, rectangular-shaped opal microchannels on a glass substrate grown by DEISA: a) low-magnification view showing a large area parallel array of opal microchannels b) the cleaved ends of the opal microchannels showing that the microspheres fill up to the top of the microchannels, c) the top view of the opal inside a microchannel showing a single domain opal with <111> top surface.

surface-tension forces between microspheres and the walls of the microchannels appear to direct microsphere crystallization entirely in these geometrically confined spaces. Figure 3b depicts the cleaved ends of the opal microchannels and Figure 3c displays the top view of the orientated crystal, which shows clear evidence for a highly ordered triangular arrangement of silica microspheres corresponding to the (111) plane of a face-centered cubic (fcc) lattice. They suggest that in the DEISA method of making opal microchannels, layers of microspheres form and pack parallel to the bottom of the substrate. We have studied the optical quality of the confined crystals by optical microspectroscopy. An example of the optical properties of a

  1616-301X/02/0706-0426 $ 17.50+.50/0

ADVANCED FUNCTIONAL MATERIALS

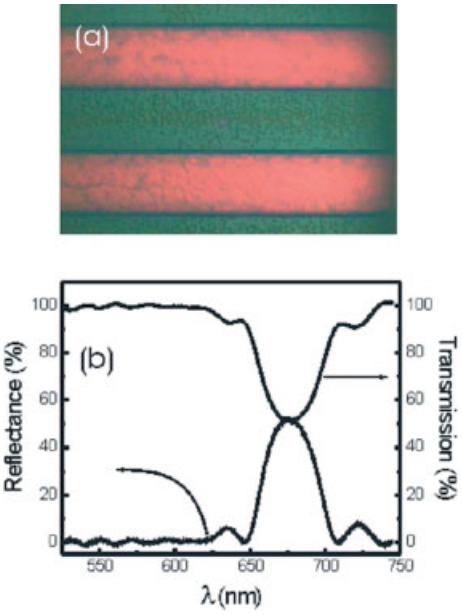

Fig. 4. a) Optical micrograph of a uniform thickness opal microchannel (channel width = 25 μm) composed of silica microspheres (diameter = 320 nm) obtained in reflection mode. The red color, corresponding to the reflectance maximum observed in the spectra, originates from the Bragg diffraction coming from the (111) planes of the confined crystal. b) Optical reflectance and transmittance spectra of the same opal microchannel. Spectra have been obtained employing a microspectroscopy technique. A spatial filter of 10 μm × 10 μm was used.

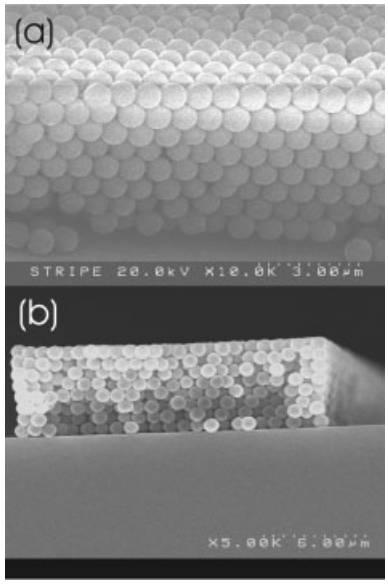

Fig. 5. Representative SEM images of a single rectangular-shaped opal prepared by the DEISA method. The sample is cleaved and the polymer dividing wall is removed by calcination in order to image the two different crystal faces: a) opal crystal plane facing towards the dividing wall, b) cleaved end of the opal crystal along the microchannel.

confined colloidal crystal made of 320 nm silica spheres is shown in Figure 4. In this case, organosilica walls were built on top of a glass substrate, allowing optical measurements to be performed in both reflection and transmission modes. The main reflectance (transmission) peak (dip) corresponds to the lowest stop band along the [111] direction of the crystal. The side fringes observed in the spectra are due to the finite size of the crystal, in good agreement with previous observations[11] and theoretical predictions.[12] A detailed study of the fluctuation of the photonic crystal properties of the confined opal crystals along the channel, as well as the effect of the crystal size and the nature of the substrate, is currently being developed. Preliminary results show that the optical quality of the confined crystals, as shown in Figure 4, is maintained for lengths on the order of hundreds of micrometers along the channel.

In order to unequivocally identify the structure and orientation of opal crystal grown in rectangular-shaped microchannels by the DEISA technique, a thorough analysis of cleaved edges of the microchannels was performed. An example of the micrographs employed for this analysis is shown in Figure 5. It can be noted that, for all samples investigated, the crystalline faces observed in different directions were only compatible with a fcc structure. The size of the opal crystals was always of the order of a few micrometers, which facilitates and enhances the accuracy and conclusions of this investigation. Based on this kind of study, it has proven possible to assign the following three main crystalline directions to the oriented opal crystals grown by DEISA with respect to the faces of the rectangular-shaped microchannels:

- the [111] crystalline direction oriented perpendicularly to the bottom of the microchannel
- the [11$\bar{2}$] crystalline direction oriented perpendicularly to the walls of the microchannel
- the [1$\bar{1}$0] crystalline direction oriented parallel to the direction of the longest dimension of the microchannel and perpendicular to the two main directions described above

This tendency of microspheres to crystallize in an fcc lattice rather than in any of the other possible close-packed structures (random or hexagonal close packed) has been observed in other kinds of microsphere ordering processes.[13,14] It has to be pointed out that even when the crystalline direction perpendicular to the channel walls is the [11$\bar{2}$], we have often observed that the opal free surface closer to the channel walls belongs to the {111} family of planes, which forms an angle of 109° with the top (111) planes instead of 90° as expected for the (11$\bar{2}$) plane. This can be seen in the cross section shown in Figure 5b, which shows explicitly that the angle between the top and the lateral surfaces is different than 90°. In the case of the present work it is believed that this phenomenon is strongly biased by the presence of vertical walls in the microchannels.

In Figure 6 a graphical representation of the opal crystal grown inside the rectangular-shaped microchannel template shows the lattice structure of the top (111), end (1$\bar{1}$0), and side (11$\bar{2}$) crystal faces of the opal microchannels. These lattice projections are superimposed on the photonic band structure of the opal at positions that correspond to the respective crystallographic directions of the opal microchannel, Figure 7. It can be seen how photon frequency stop bands open in some of these directions, which may have an optical filtering effect or selective influence upon light propagating through or impinging on to the opal microchannel and therefore can likely be put into practice in actual microphotonic crystal optical devices.

  1616-301X/02/0706-0427 $ 17.50+.50/0

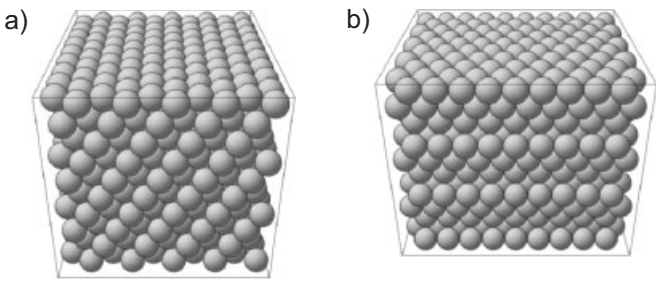

Fig. 6. A graphical representation of the opal crystal grown inside the rectangular-shaped microchannel, a) the $(1\bar{1}0)$ face of the opal crystal running along the microchannel and b) the $(11\bar{2})$ face of the opal crystal facing the dividing wall.

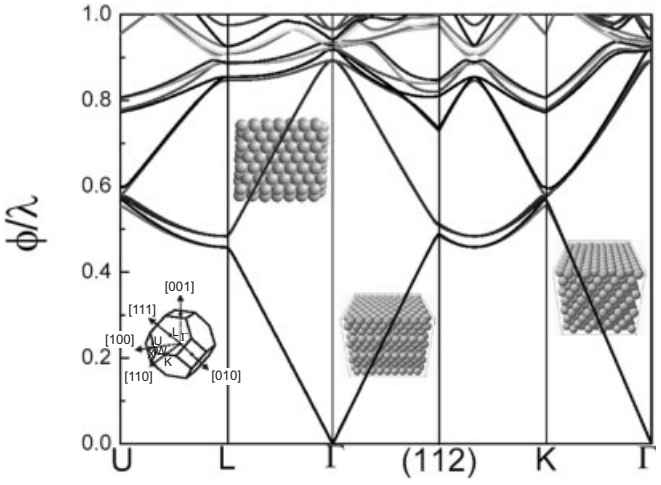

Fig. 7. The photonic band structure of the opal crystal showing the points of the Brillouin zone corresponding to the main crystallographic directions of the opal microchannel.

2.3. Assisted Directed Evaporation-Induced Self-Assembly (ADEISA)—Large Sphere Opal Microchannel

DEISA works very well for microsphere diameters ranging from 100–500 nm. The upper limit is due to the deleterious effects of rapid gravity-driven sedimentation of colloidal spheres. We modify the DEISA process by adding a spinning magnetic bar at the bottom of the container so that the spheres are maintained in a levitated state by hydrodynamic forces in the solvent as illustrated in Figure 8. We called this assisted directed evaporation-induced self-assembly (ADEISA). The novelty of ADEISA is to maintain large diameter silica microspheres (700 nm to 2500 nm) in a liquid dispersion and not allow them to suffer from too rapid sedimentation by gently stirring the dispersion of microspheres at a controlled rate. To expand, a rectangular-shaped microchannel patterned template is immersed in an ethanolic dispersion of silica microspheres (diameter 850 ± 20 nm, microsphere loading in ethanol 1–5 wt.-%) in a 30 mL vial (2.5 cm diameter and 8 cm long). The dispersion is slowly agitated by magnetic stirring at a rotation rate of 100 rpm to 300 rpm so that the solution meniscus is maintained in a quiescent state. In the region of the meniscus contacting the patterned substrate, a combination of evaporation-induced

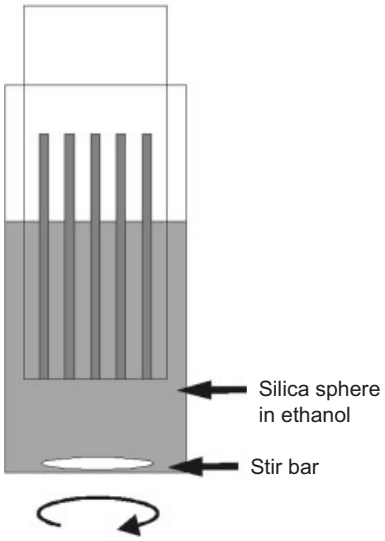

Fig. 8. A graphical representation of the experimental set-up of ADEISA.

self-assembly and mass transport, hydrodynamic and capillary forces cause the large diameter silica microspheres to crystallize exclusively within the microchannel spaces and not on the top surface of the dividing microchannel walls.

In the ADEISA method it is not immediately obvious that microsphere agitation would work because it is counter-intuitive to the criteria that need to be satisfied in the formation of well-ordered opals; however, very surprisingly it works well as shown in Figure 9, which depicts opal microchannels made

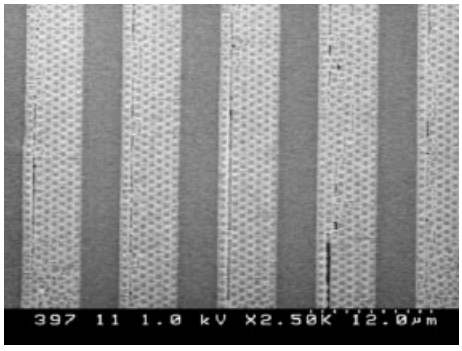

Fig. 9. Representative SEM image of a parallel array of micrometer-scale, rectangular-shaped opal microchannels composed of 850 nm silica spheres grown by ADEISA on a glass substrate.

of 850 nm silica microspheres by the ADEISA method described above. This method works very well for large monodisperse silica microspheres (700 nm to 2500 nm), which is a pivotal length scale for making silicon and germanium photonic crystals with complete photonic bandgaps for perceived applications in the near-infrared optical telecommunication wavelength range.[15–17] Clearly, microsphere agitation, by mechanical, acoustical, or thermal means of a quiescent dispersion of microspheres in ethanol serves to maintain microspheres in a state of levitation whereby they undergo enhanced microsphere collisions but without disturbing the quiescent state of the meniscus. This favorable situation works cooperatively with

  1616-301X/02/0706-0428 $ 17.50+.50/0

ADVANCED FUNCTIONAL MATERIALS

capillary forces and mass-transport effects to drive the microspheres into the channels and away from the upper surfaces of the dividing walls and enables efficient self-assembly, ordered, and oriented growth of large diameter microspheres exclusively localized within the microchannels instead of allowing them to settle too quickly under gravity-driven sedimentation, which would prevent colloidal crystallization within the spatial confines of the microchannels.

2.4. Opal Microchannels—Modulated Thickness

The method for fabricating modulated thickness opal microchannels with vertical walls and rectangular cross section is illustrated in Figure 10. Two PDMS masters with a pattern of parallel rectangular-shaped microchannels are placed face-to-face with the microchannels oriented orthogonally with respect to each other. A photocurable polymethacrylate (PMA, SK-9, Summers optical) is infiltrated into the microchannels driven by capillary effect. After curing under UV for an hour, one PDMS stamp is careful removed leaving a log-pile structure on the other PDMS stamp. This stamp is then hot-pressed (180 °C, 1 kg cm^{-2}, 5–8 h) on a glass substrate. During the thermal treatment, the PMA line structure imprints its pattern onto the PDMS stamp, which is then carefully peeled off. The imprinted PDMS stamp is used for microtransfer molding (microTM) to form a microchannel template with rectangular cross section and modulated steps on a flat substrate. This patterned substrate is then dipped into an ethanolic dispersion of silica microspheres and the microspheres deposit and self-assemble into opal microchannels with modulated thickness through DEISA or ADEISA. Since the periodic steps inside the microchannel are 1 μm deep, we believe there is no detrimental effect on the solution meniscus inside the microchannels and subsequently on opal microchannel formation.

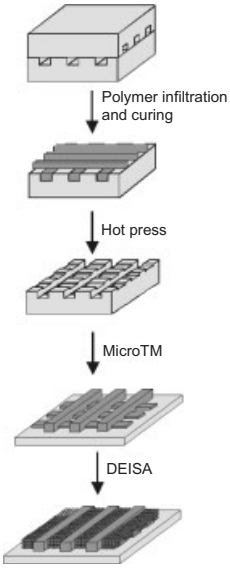

Fig. 10. Schematic diagram showing the fabrication of opal-modulated microchannel architectures on patterned substrates.

Concerning the optical properties of such a structure, Figure 11 shows optical micrographs of a modulated thickness opal microchannel made of 315 nm silica microspheres. Figure 12 displays a set of reflectance spectra that have been measured employing an optical microscope spectroscopy technique and correspond to six consecutive square opal crystal tiles as those shown in Figure 11. A square spatial filter of 10 μm × 10 μm was used to select the desired area of the modulated thickness opal crystal. The two kinds of opal crystal sites that were alternately measured are labeled as 1 and 2 in Figure 11B. The effect of opal crystal size on the width of the main peak as well as on the number and spectral separation of the secondary minima observed in the reflectance spectra can clearly be seen in Figure 12 and is found to agree closely with that predicted by theoretical calculations based on the scalar wave approximation.[18] For comparison, the spectra calculated using this approximation and corresponding to the two different opal crystal sizes (namely, 18 and 21 close-packed sphere layers) present

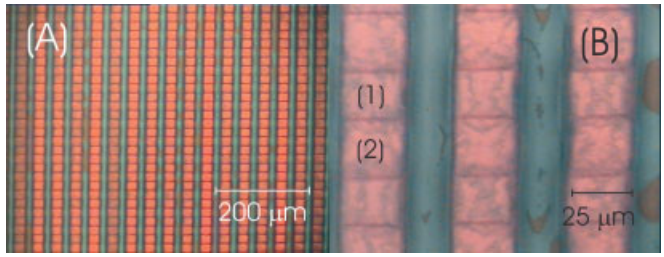

Fig. 11. Optical micrographs of modulated thickness opal microchannel: A) × 100 and B) × 500. The red color is due to the [111] Bragg diffraction of the opal crystal confined inside the microchannel. The tile-like pattern is due to the periodic steps inside the microchannel. Labels (1) and (2) correspond to the thick and thin confined colloidal crystal tiles, respectively.

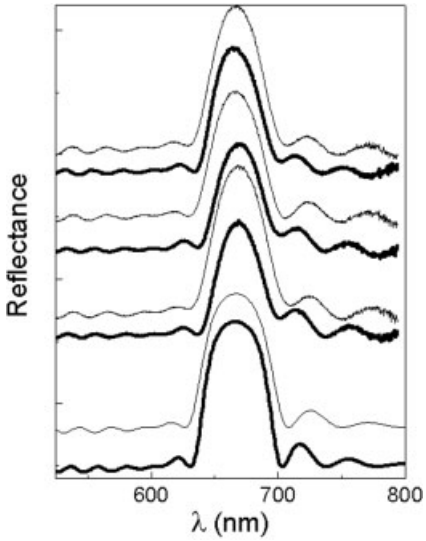

Fig. 12. Optical reflectance spectra of six consecutive opal crystal tiles of different thickness. Spectra plotted using a thick line were obtained from sites like those labeled as (1) in Figure 11 and which present a crystal thickness of close-packed layers with 21 microsphere. On the other hand, thin-line spectra correspond to the smaller thickness, 18 layers, opal crystal sites labeled as (2). Spectra calculated using a 1D scalar wave approximation in which the finite size of the crystals is taken into account are also shown (two plots at the bottom of the graph). A clear periodic modulation of the photonic crystal properties is observed.

  1616-301X/02/0706-0429 $ 17.50+.50/0

in the opal microchannel are shown at the bottom of Figure 12. The ratio of the spectral separation between the two reflectance minima defining the primary reflectance maximum and the position of this maximum shows a clear periodic oscillation between 10 % and 12 % for thick and thin crystalline regions, respectively. This explicitly demonstrates the controlled modulation of the photonic crystal properties.

2.5. Opal Microchannels—Modulated Lattice Dimension

An amalgamation of the DEISA/ADEISA techniques and microsphere self-assembly inside rectangular-shaped microchannels has been utilized to create a modulated lattice-dimension opal microchannel heterostructure, which may be used as a bi-frequency optical Bragg mirror or a tunable width single frequency optical Bragg filter. The fabrication process is depicted in Figure 13. A PDMS stamp patterned with rectangular-shaped microchannels is placed into conformal contact

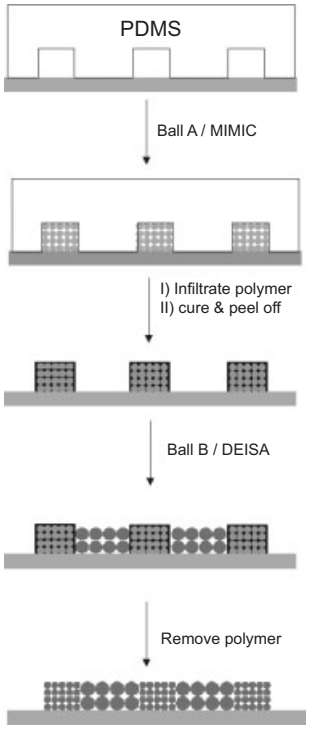

Fig. 13. Schematic illustration showing the fabrication of a modulated lattice dimension opal heterostructure.

with a flat substrate (glass, quartz, Si wafer, or polymer sheet). A 1–3 wt.-% dispersion of colloidal silica microspheres (diameter = 550 ± 20 nm) in a water/ethanol mixture (4:1, v/v) is added to one end of the microchannel.[19] Microspheres, driven by capillary forces, move into the rectangular-shaped microchannels. Evaporation of solvent from the other end of the microchannels drives a flux of microspheres into the end of the microchannel, which induces the self-organization of the microspheres and ultimately leads to a close-packed, well-ordered opal crystal. The opal crystals confined in the PDMS microchannel template are dried in a desiccator. A UV-curable polyurethane is then infiltrated into the void space of the confined opal crystal driven by capillary forces. After curing under UV light for 4 h the PDMS is peeled off to leave a rectangular-shaped microchannel pattern on the substrate, in which the wall is composed of a matrix of silica opal and polyurethane. This patterned composite substrate is then immersed into an ethanolic dispersion of larger diameter silica microsphere (diameter = 970 nm, 0.5–1 wt.-%). The microspheres are deposited inside the microchannels through ADEISA. The embedded polyurethane is removed by calcination at 450 °C for 5 h.

A representative scanning electron microscopy (SEM) image is shown in Figure 14a for an opal microchannel heterostructure with modulated lattice dimensions that have been pre-

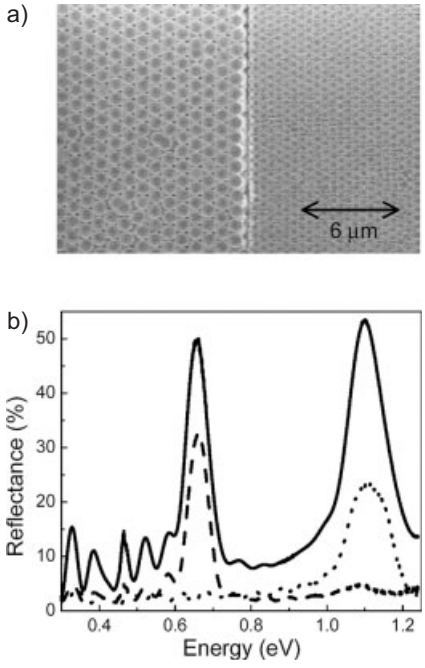

Fig. 14. a) Representative SEM image of an opal microchannel heterostructure composed of 550 nm and 970 nm silica spheres; b) micro-optical reflectance spectra of the same structure showing the reflectance corresponding to the individual arrays of single sphere size-confined crystals (dashed and dotted lines) and the alternating sphere size-confined crystal heterostructure (solid line).

pared by the same procedure as above. The sequence of microsphere infiltration plays an important role in the degree of ordering of microspheres in the opal microchannel heterostructure. The overall quality of the opal microchannel crystals and their interfaces are better in the case of small-sphere infiltration, followed by large-sphere DEISA. It is believed that the improvement in the opal crystal order is due to a smoother surface of a small microsphere–polymer nanocomposite wall than that of a big microsphere–polymer nanocomposite wall for the DEISA process. Figure 14b shows optical reflectance measurements of the corresponding structure comprised of alternating planarized opal microchannels made of 550 nm and 970 nm diameter microspheres. The optical reflectance of each one of the two different microchannel arrays comprising the opal heterostructure are shown—dashed and dotted line for

  1616-301X/02/0706-0430 $ 17.50+.50/0

ADVANCED FUNCTIONAL MATERIALS

the larger and smaller microsphere opal microchannels, respectively. Also, the overall reflectance of the heterostructure was collected (solid line). It can be seen that the optical properties of the photonic crystal heterostructure is the result of adding up the optical properties of the individual photonic crystal components. Actually, it behaves as a bi-frequency selective tunable optical Bragg mirror in which the positions and the width of each one of the reflected frequency bands can be determined by the microsphere diameter and the physical dimensions of the opal microchannels. Alternatively, this kind of opal microchannel heterostructure can be seen to function as a mono-frequency selective tunable optical Bragg filter in which the width of the transmitted frequency band will be determined by the difference between the diameters of each kind of microsphere in the heterostructure.

3. Conclusions

While it is beyond the scope and objectives of this paper it is clear that numerous potentially useful planarized and optically integrated microphotonic crystal devices for optical telecommunication applications may be produced using the methods described in this paper for making high-quality opal architectures with complex form and designed optical functionality. These may include passive opal-based devices such as spectral filters and mirrors, wavelength division multiplexers and demultiplexers, waveguide splitters and combiners, interleavers, attenuators, wavelength dispersion compensators, and high-Q resonators. Active components such as liquid crystals and luminescence guests may also be incorporated into the components of opal-based microphotonic crystal optical circuits to achieve for example electrooptical modulation and wavelength tuning of photonic crystals, electrically and optically excited photonic crystal microlasers, and thermally tuned photonic crystal resonant structures.

Opal circuits of light based on planarized microphotonic crystals made by directed self-assembly—a fusion of microsphere crystallization and templated assembly—now seems to be a realistic and attainable goal.

4. Experimental

A glass or silicon wafer substrate is cleaned by piranha solution for 20 min and washed with copious amount of water. A PDMS stamp (Sylgard 184, Corning) is made by replica molding over a photolithographic patterned wafer. Monodisperse silica spheres are prepared by the Stöber method [20].

Micromolding inside Microcapillaries (MIMIC): A PDMS stamp is placed into conformal contact with a substrate, such as a glass slide or silicon wafer. A drop of silica sol (mixture of tetramethoxysilane and 0.1 N oxalic acid (3:1, w/w), organic modified silica sol (mixture of 3-(glycidoxypropyl) trimethoxysilane, tetramethoxysilane, and 0.1 N oxalic acid, 5:1:1, w/w) [21] or pre-polymer (NOA-73 from Norland or F301 from Epotek) is infiltrated into the microchannels. The sol spontaneously polymerizes and solidifies in two days and the pre-polymer cures by exposure to UV light in 1 h (Norland) or annealing at room temperature for 18 h (Epotek). The PDMS stamp is then peeled off the substrate to create a pattern of vertical wall and flat bottom parallel microchannels.

Wet Chemical Etching of Si(100): A line-patterned PDMS is inked with hexadecanethiol (2 mM) solution by using a cotton swab, followed by drying under a N_2 stream for 30 s. The stamp is then put into contact for 5–10 s with a 50 nm Au/5 nm Ti coated Si(100) wafer. The titanium layer is used to promote adhesion. In the printing step, the line pattern is oriented at 45° with respect to the flat end of the wafer. After printing, the bare gold is etched by 1 M KOH/0.1 M $K_2S_2O_3$/0.01 M $K_3Fe(CN)_6$/0.001 M $K_4Fe(CN)_6$ for 15 min. The underlying Ti is removed by 1 % HF for 1 min. The silicon is then anisotropically etched by a KOH solution (60–70 g KOH, 30–40 g H_2O, 20 mL 2-propanol). The remaining gold and titanium are removed by aqua regia.

Deep RIE of Si(100): A layer of SiO_2 (ca. 0.8 μm thick) is thermally grown on a Si(100) wafer at 900 °C. A line photoresist pattern (HPR504, thickness 1.5 μm) is formed by photolithography. The exposed SiO_2 is etched by a buffered hydrofluoric acid bath for 15 min and then the photoresist is stripped off by acetone. DRIE is performed on the patterned wafer inside an Oxford RIE instrument. Each cycle of the Bosch process involves two steps, an etch step of silicon by SF_6 gas followed by a C_4F_8 deposition step on the silicon surface. The etch rate is ca. 0.5 to 0.8 μm per cycle. The deposited fluorinated material was finally removed by a hot piranha solution to yield the desired silicon surface relief pattern of parallel microchannels with a rectangular cross section.

Modulated Thickness Channel: Two line-patterned PDMS stamps are put face-to-face orthogonally to each other. The log-pile array is filled with a photocurable polymethacrylate (SK-9, Summers Optical) by the capillary effect. After curing under UV for one hour, one PDMS stamp is careful removed leaving a log-pile structure on the other PDMS stamp. This stamp is then hot-pressed (180 °C, 1 kg cm^{-2}, 5–8 h) onto a flat substrate (glass, quartz, or Si wafer). During the hot-press step, the PMA line structure imprints its pattern on the PDMS stamp. A drop of UV curable polyurethane (NOA73, Norland) is added to this imprinted PDMS stamp and the excess is removed by a flat PDMS stamp. The stamp is then put into conformal contact with a flat substrate (e.g., glass, Si wafer, or polymer sheet). After curing under UV light for 4 h the PDMS is peeled to leave a flat microchannel template with rectangular cross section and modulated steps.

Received: January 31, 2002
Final version: April 8, 2002

[1] S. John, *Phys. Rev. Lett.* **1987**, *58*, 2486.
[2] E. Yablonovitch, *Phys. Rev. Lett.* **1987**, *58*, 2059.
[3] V. L. Colvin, *MRS Bull.* **2001**, *26*, 637.
[4] a) S. M. Yang, G. A. Ozin, *Chem. Commun.* **2000**, 2507. b) G. A. Ozin, S. M. Yang, *Adv. Funct. Mater.* **2001**, *11*, 95.
[5] Y. Yin, Y. Lu, B. Gates, Y. Xia, *J. Am. Chem. Soc.* **2001**, *123*, 8718.
[6] T. Ochiai, J. Sánchez-Dehesa, *Phys. Rev. B* **2001**, *64*, 245 113.
[7] M. N. Shkunov, Z. V. Vardeny, M. C. DeLong, R. C. Polson, A. A. Zakhidov, R. H. Baughman, *Adv. Funct. Mater.* **2002**, *12*, 21.
[8] J. D. Joannopoulos, P. R. Villeneuve, S. Fan, *Nature* **1997**, *386*, 143.
[9] Y. Xia, G. M. Whitesides, *Annu. Rev. Mater. Sci.* **1998**, *28*, 153.
[10] O. Powell, H. B. Harrison, *J. Micromech. Microeng.* **2001**, *11*, 217.
[11] J. F. Bertone, P. Jiang, K. S. Hwang, D. M. Mittleman, V. L. Colvin, *Phys. Rev. Lett.* **1999**, *83*, 300.
[12] K. W. K. Shung, Y. C. Tsai, *Phys. Rev. B* **1993**, *48*, 11 265.
[13] H. Miguez, F. Meseguer, C. Lopez, A. Mifsud, J. S. Moya, L. Vazquez, *Langmuir* **1997**, *13*, 6009.
[14] P. Jiang, J. F. Bertone, K. S. Hwang, V. L. Colvin, *Chem. Mater.* **1999**, *11*, 2132.
[15] A. Blanco, E. Chomski, S. Grabtchak, M. Ibisate, S. John, S. W. Leonard, C. Lopez, F. Meseguer, H. Miguez, J. P. Mondia, G. A. Ozin, O. Toader, H. M. van Driel, *Nature* **2000**, *405*, 437.
[16] H. Miguez, E. Chomski, F. Garcia-Santamaria, M. Ibisate, S. John, C. Lopez, F. Meseguer, J. P. Mondia, G. A. Ozin, O. Toader, H. M. van Driel, *Adv. Mater.* **2001**, *13*, 1634.
[17] Y. A. Vlasov, X.-Z. Bo, J. C. Sturm, D. J. Norris, *Nature* **2001**, *414*, 289.
[18] H. Miguez, S. M. Yang, G. A. Ozin, *Appl. Phys. Lett.*, in press.
[19] E. Kim, Y. Xia, G. M. Whitesides, *Adv. Mater.* **1996**, *8*, 245.
[20] W. Stober, A. Fink, E. Bohn, *J. Colloid Interface Sci.* **1968**, *26*, 62.
[21] O. J. A. Schueller, G. M. Whitesides, J. A. Rogers, M. Meier, A. Dodabalapur, *Appl. Opt.* **1999**, *38*, 5799.

  1616-301X/02/0706-0431 $ 17.50+.50/0